Characterizing irradiated surfaces using IR spectroscopy

Rosario Brunetto, C. Lantz, T. Nakamura, D. Baklouti, T. Le Pivert-Jolivet, S. Kobayashi, F. Borondics

Version of Record: https://www.sciencedirect.com/science/article/pii/S0019103520301135
Manuscript_91e8d7341fc1a957328b968a9bb38780

Characterizing irradiated surfaces using IR spectroscopy

R. Brunetto[1], C. Lantz[1], T. Nakamura[2], D. Baklouti[1], T. Le Pivert-Jolivet[1], S. Kobayashi[2], F. Borondics[3]

[1]Université Paris-Saclay, CNRS, Institut d'Astrophysique Spatiale, 91405, Orsay, France (rosario.brunetto@ias.u-psud.fr)
[2]Division of Earth and Planetary Materials Science, Graduate School of Science, Tohoku University, Japan
[3]SOLEIL synchrotron, Gif-sur-Yvette, France

Abstract

Solar wind ion irradiation continuously modifies the optical properties of unprotected surfaces of airless bodies in the Solar System. This alteration induces significant biases in the interpretation of the spectral data obtained through remote sensing, and it impedes a correct estimation of the composition of the sub-surface pristine materials. However, as the alteration of the surface is a function of time, an in-depth understanding of the phenomenon may provide an original way to estimate the weathering age of a surface. Laboratory experiments show that mid- and far-IR bands are very sensitive to space weathering, as they are significantly modified upon irradiation. These bands can thus constitute a reliable proxy of the time-bound effects of irradiation on an object. We show that the detection of irradiation effects is within the reach of IR spectral resolution of the OSIRIS-REx mission and of the future James Webb Space Telescope. Our results provide a possible evidence for space weathering effects in the IR spectrum of asteroid 101955 Bennu measured by OTES/OSIRIS-REx.

1. Introduction

The remote sensing observations of Solar System airless bodies deal with the problem of the surfaces being constantly modified by exogenous alterations. For bodies in the inner Solar System, slow solar wind ion irradiation and micrometeoroid impacts are driving the alteration of airless surfaces, with solar wind dominating the alteration across most surface types (Brunetto et al. 2015). Even if slow solar wind ions penetrate the surface less than 1 µm, they significantly affect the optical properties of the upper layers (Noguchi et al. 2014; Bonal et al. 2015; Loeffler et al. 2009) which are the ones probed by the remote sensing observations. Microstructural/chemical modifications by solar wind irradiation may include the production of disordered rims (amorphous or partly amorphous), implantation vesicles, solar flare tracks, nanophase-Fe-bearing particles, which all contribute to some extent to the alteration of surface spectral properties. As we induce the composition of the bulk of the object from the observation of the upper layers, the irradiation may seriously affect the spectral identification of underlying pristine materials. The resulting biases hamper both the

understanding of the spectral diversity of small bodies and their link to extraterrestrial materials available in our laboratories.

The ion irradiation of surface regolith is known to be particularly intense on the Moon (Hapke 2001). However, asteroid surfaces are on average much younger than the Moon's "undisturbed" terrains and their regolith has a much higher mobility due to the low gravity. So it was remarkable to observe that even young asteroid families show clear effects of surface aging (Vernazza et al. 2009). As a matter of fact, the solar wind fluxes in the inner Solar System are so intense that the astrophysical time necessary to produce any modification of the asteroid surfaces is lower than 1 Myr (Strazzulla et al. 2005; Hapke 2001). This was confirmed by the laboratory analysis of samples collected from the young surface of the asteroid Itokawa by the Hayabusa mission. The Itokawa grains showed incipient space weathering effects (Noguchi et al. 2011), with the presence of disordered rims resulting from solar wind radiation damage (Noguchi et al. 2014; Keller and Berger 2014), and with the presence of solar flare tracks. Exposure ages estimated through the analysis of the solar flare track densities (calibrated for 1AU using lunar samples) were in the range 10^3-10^6 years, depending on the considered particle (Noguchi et al. 2014; Nagao et al. 2011).

Despite being a complicated source of spectral biases, surface weathering could provide a convenient tool to estimate the age of a young surface. The direct measurements of the exposure time of surface materials is currently only possible thanks to the laboratory analysis of samples collected and returned from space (Nagao et al. 2011) (e.g., the unique cases of Itokawa and the Moon, and soon asteroids Ryugu and Bennu). The remote sensing spectroscopy of irradiated surfaces can provide an additional aging chronometer, independent from the timescales derived from dynamical studies (Brunetto et al. 2006). We thus have two good reasons to study how space weathering modifies the reflectance spectra of airless surfaces: to remove the biases affecting remote sensing and to estimate the age of the surface. However, it is mandatory to first establish reliable spectral proxies for distinguishing an irradiated from a pristine surface. These criteria must be based on unambiguous and reproducible spectral variations upon irradiation.

In the case of bright objects, the irradiation of exposed surfaces has mainly been studied by detecting the spectral variations induced by weathering agents (energetic ions, micrometeorites) in the visible and near-IR range (VIS-NIR, 0.4-2.5 µm), both through direct observations (Binzel et al. 2004) and simulation experiments (Sasaki et al. 2001). Typical spectral variations included changes in the spectral slopes and reflectance (Marchi et al. 2005). These variations have been largely documented since the '70s in the case of the Moon (Pieters et al. 1993), and since the '90s for bright asteroids (Binzel et al. 2004; Marchi et al. 2005). For S-type asteroids, the reddening of the VIS-NIR spectral slope proved to be a good proxy of space weathering.

Unlike the case of bright objects such as S-type asteroids, a clear and univocal VIS-NIR weathering trend cannot be established in the case of the more numerous dark asteroids (Nesvorný et al. 2005; Lazzarin et al. 2006). In previous work, we found that dark carbon-rich meteorites of various compositions showed different VIS-NIR spectral trends after ion irradiation (Lantz et al. 2017). In addition, the VIS-NIR spectral slopes and albedo are known to be influenced by several factors other than composition, such as surface porosity, grain size and roughness. In the case of dark objects, these parameters induce VIS-NIR spectral

variations that in some cases are comparable to or larger than the weathering trends (Lantz et al. 2015). For all these reasons, an unambiguous spectral weathering trend for primitive objects cannot be determined using VIS-NIR data alone (Lantz et al. 2017). Additional information is required from other spectral ranges with diagnostic bands, such as the mid-IR (MIR, 2.5-17 µm) and far-IR (FIR, 17-100 µm) ranges.

In previous studies (Lantz et al. 2015, 2017; Brunetto et al. 2014), we reproduced the solar wind weathering of primitive asteroids in the laboratory, by irradiating a number of carbonaceous chondrites from different sub-classes (including CM Murchison and Mighei, CO Lancé and Frontier Mountain 95002, CI Alais, CV Allende, and C2 Tagish Lake) with He^+ ions. We studied the laboratory-irradiated samples using reflectance spectroscopy and more recently micro-spectral imaging (Brunetto et al. 2018). Ion irradiation of the meteorites induced significant IR spectral variations. A comparison of the spectral imaging data at different wavelengths demonstrates that IR photons from the center of the reststrahlen bands (surface scattering) are significantly more efficient in detecting irradiated areas on the sample than visible photons and IR photons in volume scattering ranges (see Appendix A and Fig. A1).

To explore to what extent the IR bands are a good proxy of irradiation, we decided to analyze our set of meteorite samples with FIR spectroscopy (in almost all our previous analyses the measured spectral range stopped at 15 µm (Lantz et al. 2017)). In this paper we report the results of these new measurements, plus a new irradiation experiment performed on a polished section of the CM2 Murchison meteorite.

2. Experimental setup

2.1 Laboratory irradiation of meteorites

The preparation of the pellets (13 mm diameter) of the CV3 Allende, CO3.5 Lancé, CO3 FM95002, CM2 Murchison, CM2 Mighei, CI1 Alais, and C2-ung Tagish Lake meteorites is reported elsewhere (Brunetto et al. 2014; Lantz et al. 2015, 2017). A new 1-cm sized chip of the CM2 Murchison meteorite with a flat surface with roughness made by a #400 polishing disk was prepared at Tohoku University in Japan. All the samples were irradiated at the SIDONIE implanter of CSNSM-Orsay (France), using He^+ ion beams with 40 keV energy (20 keV for the Murchison chip), at ion flux of ~10^{13} ions/(sec cm^2) up to a total fluence of ~$6x10^{16}$ ions/cm^2. The samples were monitored in situ under vacuum by VIS-NIR diffuse reflectance spectroscopy. Details of the irradiation conditions are described in our previous studies (Brunetto et al. 2014; Lantz et al. 2015, 2017).

2.2 IR spectroscopy

The FTIR hyperspectral imaging measurements reported in Fig. A1 were acquired with an Agilent Cary 670/620 micro-spectrometer equipped with a 128x128 pixel Focal Plane Array detector, installed at the SMIS beamline of the SOLEIL synchrotron (France). Mid-IR spectra were measured using the internal globar source at 8 cm^{-1} spectral resolution. The infrared maps were acquired in reflectance geometry, with respect to gold references. More details can be found elsewhere (Brunetto et al. 2018). The MIR part of the spectra reported in

Section 3 was measured in a previous study (Lantz et al. 2017) using a spectral resolution of 4 cm^{-1}.

The new FIR spectra reported in this study (Figs. 1-3) were acquired at the SMIS beamline using a NicPlan microscope, coupled to a iS50 FTIR spectrometer (Thermo Fisher) operating in confocal reflection geometry, with respect to gold references. To measure in the far-IR range (700–100 cm^{-1} or 14–100 µm), we used a bolometer detector (boron doped silicon, 4.2 K cooled, Infrared Laboratories) and a solid-state Si beamsplitter. The spectral resolution was 4 cm^{-1} (constant in wavenumber, but variable in wavelength, typically ~0.16 µm in the 20 µm region and ~0.98 µm in the 50 µm region) and the spectral sampling 0.5 cm^{-1} (typically ~0.02 µm in the 20 µm region and ~0.125 µm in the 50 µm region). We analyzed irradiated and unirradiated areas on each sample, using spot sizes of about 300 µm in diameter per spectrum. The various spectra (typically 5 spectra per meteorite) of the unirradiated spots were averaged, as well as the irradiated spots, to finally produce average spectra representative of the unirradiated and irradiated meteorites. Thus, we averaged the small scale heterogeneity of the chosen chondrites. The bolometer also allowed us to acquire data in the 750-1050 cm^{-1} (13.3-9.52 µm) range. Although noisy, this additional spectral range proved to be extremely useful to properly combine spectral ranges obtained with different detectors (see Fig. 2). The FIR spectra were scaled to match the MIR spectra in the overlapping region. The combined MIR-FIR spectra were then baseline corrected using a convex hull. The baseline correction was performed to focus on the position and shape of the IR spectral bands, and to allow comparison with IR remote sensing data of asteroids whose continuum is usually taken into account and removed in the thermal model of the spectral energy distribution (Emery et al. 2006). We calculated the peak positions of the IR bands from the 1st derivative of the spectra (Table 1) and the error is estimated based on the spectral sampling and the noise in the data (increasing with decreasing wavenumber). A similar procedure to determine the peak positions was applied to remote sensing data of Bennu and Hektor asteroids (see Section 4) and an additional double-check was obtained from polynomial fits around the center of the bands.

In our microscopes we used Schwarzschild objectives, which accept photons in a large range of angles at all azimuths. The geometry of the spectral measurements can influence the spectral shape (Salisbury et al. 1991; Salisbury 1993), thus a direct comparison between reflectance and emissivity spectra must be taken with great care. In this paper we do not try to necessarily find the best laboratory match to asteroid spectral data, but we rather focus on relevant modifications of spectral features induced by ion irradiation.

Irradiation experiments and IR spectral measurements were performed in two different laboratories, and the spectra were measured ex situ in laboratory air. Potential air-exposure effects such as oxidation cannot be excluded. However, if present, they do not seem to have any significant effect over time on the spectral modifications shown here, as we have verified by comparing the FIR spectra obtained on Allende in the new measurements with one Allende FIR spectral measurement reported in our previous work (Brunetto et al. 2014).

3. Results

3.1 FIR spectral effects of He implantation in carbonaceous chondrites

We report in Fig. 1 the new laboratory spectra of virgin and irradiated meteorites measured in the FIR range. In Fig. 2 we illustrate the combination of FIR and MIR ranges, as described in Section 2.2, with the examples of a meteorite whose matrix is rich in hydrated minerals (C2-ung Tagish Lake) and a meteorite whose matrix is rich in anhydrous phases (CO3 FM95002). The full collection of combined MIR-FIR spectra will be available at the DAYSY spectral database hosted by the SSHADE (Schmitt et al. 2018) Solid Spectroscopy database infrastructure (www.sshade.eu).

Different classes of carbonaceous chondrites have different IR spectra (Salisbury et al. 1991; Beck et al. 2014; Vernazza et al. 2017; Hamilton et al. 2018, 2019). Just like the MIR range is characterized by the strong Si-O stretching bands in silicates, the FIR range is dominated by the bending vibrations of the Si-O bonds and translation modes of metal ions (Jäger et al. 1998). Both MIR and FIR are thus very sensitive to the composition of the silicates and the thermal history of the meteorites (Beck et al. 2014). Our analysis confirms that the FIR spectra of meteorites whose matrix is rich in anhydrous phases (CV3 Allende, CO3.5 Lancé, CO3 FM95002) and those that are rich in aqueously altered phases (CM2 Murchison, CM2 Mighei, CI1 Alais, and C2-ung Tagish Lake) are significantly different.

Significant differences are also observed when comparing spectra before and after He^+ irradiation. The spectra of Frontier Mountain 95002 and Lancé are very similar and they both show typical olivine bands corresponding to a composition of Fo~50-60, estimated based on literature data of olivine (Hamilton 2010). After irradiation, the bands are shifted to peak positions that are observed in olivines with Fo~30-35. Similar Fo values are found based on the MIR bands, both before and after irradiation (Lantz et al. 2017). The spectra of Alais and Tagish Lake share some similarities in the 450-500 cm^{-1} (20-22.2 µm) region, but they differ significantly for wavenumbers below 400 cm^{-1} (above 25 µm), both before and after irradiation. Finally, the spectra of Murchison and Mighei also share many similarities (both are CM chondrites). Overall, almost all bands are modified by irradiation, either in terms of shape/intensity and/or in terms of peak position.

It is particularly interesting to observe how the relative intensity of the doublets observed at about 500 cm^{-1} (20 µm) and 400 cm^{-1} (25 µm) in CO/CV and at about 450 cm^{-1} (22.2 µm) in CI/C2 are modified by irradiation. Upon irradiation, the left band of these doublets is always reduced in intensity with respect to the right band. It is obvious on the 450 cm^{-1} (22.2 µm) doublet (typical of saponite (Beck et al. 2014)) of Alais and Tagish Lake, and on the low wavenumber bands of FM95002 and Lancé whose relative intensities change in a very similar way after irradiation. The ratio in relative intensity (I_left band / I-right band) before irradiation is about 1.47 for FM95002, 1.69 for Lancé, 1.01 for Tagish Lake, and 1.02 for Alais. After irradiation the ratio is about 1.09 for FM95002, 1.08 for Lancé, 0.91 for Tagish Lake, and 0.94 for Alais. The relative reduction upon irradiation is thus about 30-40% for FM95002 and Lancé and about 10% for Tagish Lake and Alais. It is interesting to observe that for almost all the considered meteorites the band near 350 cm^{-1} (28.6 µm) also increases in relative strength compared to bands at higher wavenumbers. Overall, the reflectance at lower wavenumbers is increasing with irradiation (see also the case of Allende in Fig. 3), and this can be due both to an increase of spectral slope (similarly to what is observed in the visible range for S-types) and to a modification of the relative intensity between lower and higher wavenumber bands. However, considering that the spectra have

been baseline corrected, we attribute the observed effect to a change in relative band intensity. In particular, from the non-normalized spectra of Fig. 2, we can clearly observe a reduction of the intensity (and partly a broadening) of the bands in the higher wavenumbers, a phenomenon which seems to be much weaker for bands at lower wavenumbers.

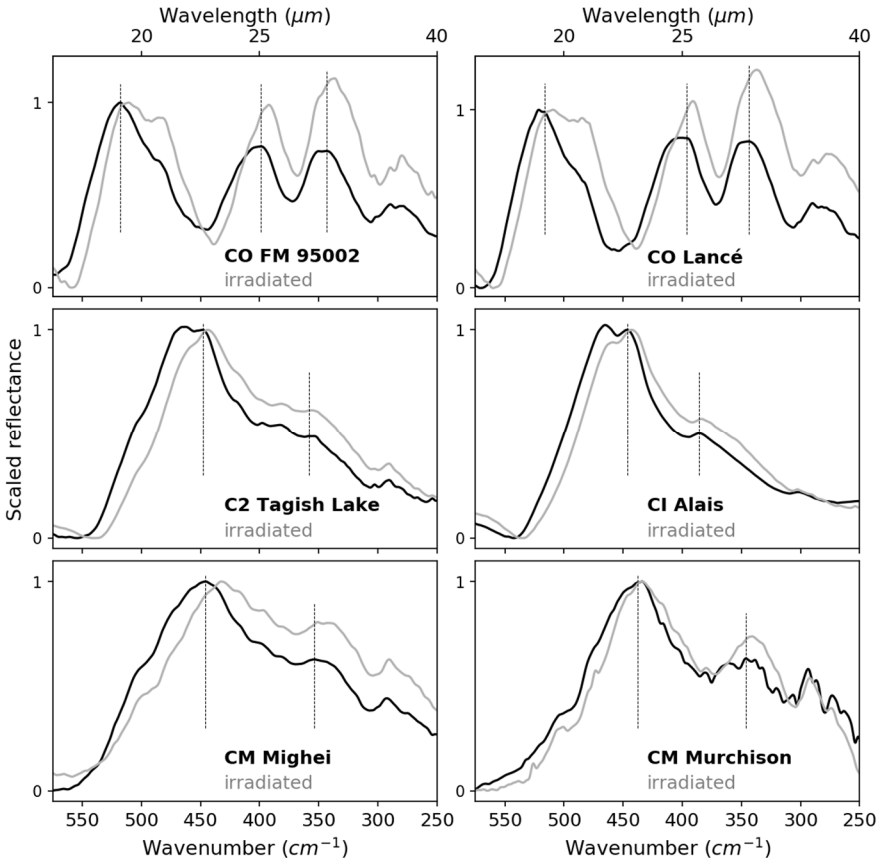

Fig. 1. FIR spectra of six meteorite samples before (black curves) and after (grey) irradiation. Frontier Mountain 95002, Lancé, Tagish Lake, Alais, and Mighei were irradiated with $6x10^{16}$ He^{+}/cm^{2} at 40 keV. Murchison spectra were acquired on a polished chip sample irradiated with $6x10^{16}$ He^{+}/cm^{2} at 20 keV. Vertical lines are drawn to guide the eye and stress the irradiation effect. The peak positions are reported in Table 1 and used in Fig. 4. All the spectra have been baseline corrected. The intensities are scaled to unity at the position of the main band before irradiation.

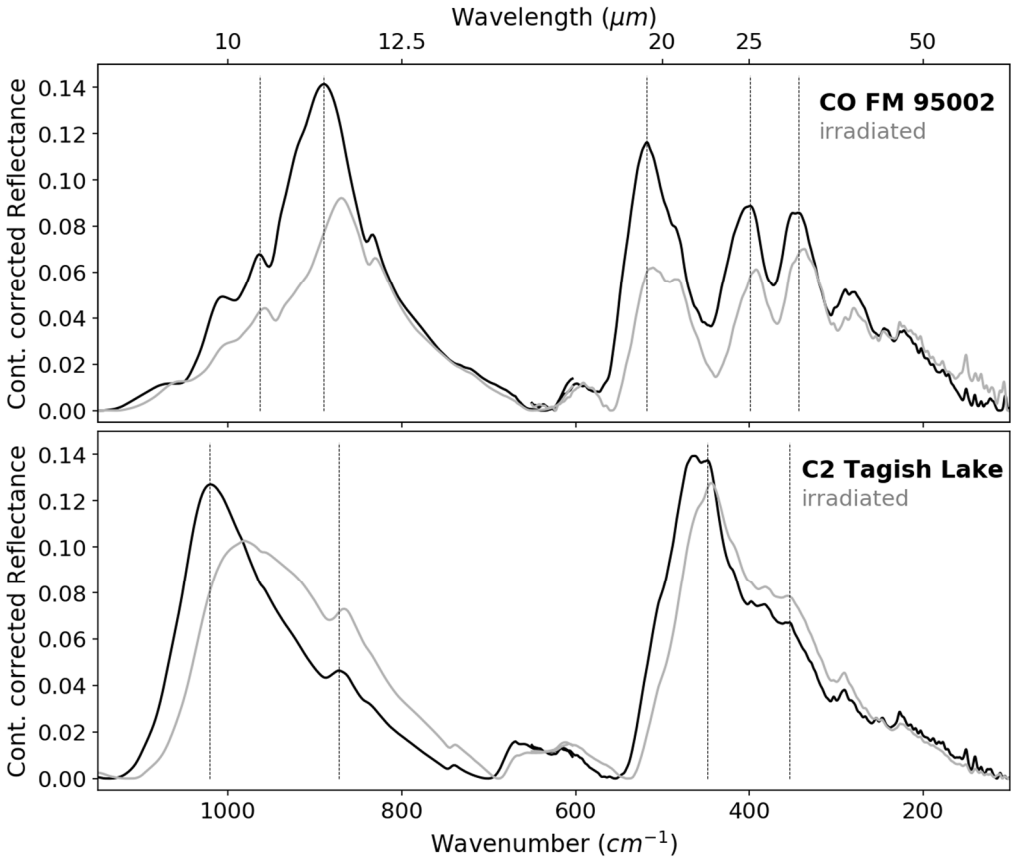

Fig. 2. Combined MIR and FIR spectra of ion irradiated carbonaceous chondrites. The continuum-removed reflectance spectra of the meteorites CO3 Frontier Mountain 95002 (top) and C2 Tagish Lake (bottom) are shown before (black curves) and after (grey) laboratory irradiation using $6x10^{16}$ He^+/cm^2 at 40 keV. The CO3 and C2 meteorites are chosen here as examples of anhydrous (Lantz et al. 2017) and hydrous (Nakamura et al. 2003) chondrites, respectively. The 830-1100 cm^{-1} (9-12 µm) and the 200-500 cm^{-1} (20-50 µm) ranges are characterized by the presence of Si-O stretching and bending vibration bands respectively. In the case of FM 95002, the bands are mainly due to anhydrous minerals (in particular olivine (Hamilton 2010)). In the case of Tagish Lake, most bands can be attributed to clay minerals (in particular saponite (Beck et al. 2014)). In this surface scattering regime, the peaks point towards the top. Vertical lines have been drawn to guide the eye along the position of the main reststrahlen bands and to stress the irradiation effect. The MIR range (1200-650 cm^{-1}) has been measured in a previous study (Lantz et al. 2017).

The silicate FIR bands are observed to shift in peak position upon irradiation. The irradiation-induced spectral shift is always observed towards the longer wavelengths (shorter wavenumbers, see Table 1), coherently with the MIR spectral shifts of the main silicate 10 µm feature observed in previous experiments on similar chondrites and on terrestrial silicates (Vernazza et al. 2013; Brunetto et al. 2014; Lantz et al. 2015, 2017). Generally speaking, the stronger the band, the larger the shift, as already observed for irradiated Allende (Brunetto et al. 2014). This is observed for all meteorites except Murchison. The shifts induced on CV and CO meteorites are very similar to each other. Also C2 Tagish Lake and CI Alais present very similar shifts after irradiation. Previous ion irradiation experiments on Tagish Lake using $1x10^{16}$ He^+/cm^2 at 200 keV reported a band shift of about 0.3 µm for the 9.8 µm (1020 cm^{-1}) band and about 0.15 µm for the 22.3 µm (448 cm^{-1}) band (Vernazza

et al. 2013), while in our case ($6x10^{16}$ He^+/cm^2 at 40 keV) the shifts are about 0.4 µm (40 cm^{-1}) and 0.2 µm (4 cm^{-1}) respectively, which could be explained by the fact that we are using a 6 times higher fluence (although at 5 times lower energy). The two CMs considered in this study behave differently from each other in terms of the shift of the main band at about 445-448 cm^{-1} (22.32-22.47 µm), with Mighei showing the largest spectral shift. While the different behavior of Mighei and Murchison might be ascribed to the different energy used in these experiments (40 and 20 keV respectively), more studies will be necessary to elucidate the dependence of the shift on the different meteorite types and/or the different ion energies.

The redshift of the main MIR and FIR bands clearly emerges as a general trend, observed in the bulk spectra of both terrestrial and extraterrestrial silicates. In addition, not only the peaks, but also the spectral minima are shifted, as for instance the minimum observed at about 450 cm^{-1} (22.2 µm) in CO/CV that shifts towards longer wavelengths after irradiation, as well as the main Christiansen features.

Meteorite	**Position before irradiation (cm^{-1})**	**Position after irradiation (cm^{-1})**	**Shift upon irradiation (cm^{-1})**
CV Allende	524 ± 1	516 ± 1	8
	393 ± 1	391.5 ± 1	1.5
	345 ± 1.5	339 ± 1.5	6
CO Lancé	516.5 ± 1	509.5 ± 1	7
	396.5 ± 1	391 ± 1	5.5
	344 ± 1.5	337 ± 1.5	7
CO FM 95002	518 ± 1	511 ± 1	7
	399 ± 1.5	392 ± 1.5	7
	343 ± 1.5	337 ± 1.5	6
CI Alais	446.5 ± 1	443 ± 1	3.5
	386 ± 1	383.5 ± 1	2.5
C2 Tagish Lake	448 ± 1	444 ± 1	4
	358 ± 1.5	356 ± 1.5	2
CM Mighei	445.5 ± 1	432 ± 1	13.5

	353.5 ± 1	350.5 ± 1	3
CM Murchison *(chip)*	438 ± 1	434 ± 1	4
	346 ± 1.5	341 ± 1.5	5

Table 1. Peak positions and shifts of the main far-IR bands of the studied meteorites. The positions are calculated from the average spectra before and after irradiation with $6x10^{16}$ He^{+}/cm^{2} (20 keV for Murchison, 40 keV for the other meteorites).

3.2 Cross section of the spectral shift upon irradiation

In the top panel Fig. 3 we report the FIR spectra of three ion irradiation experiments on Allende. The three virgin pellets have similar spectra in terms of shape and band position, which confirms that we are averaging the small scale heterogeneity of the meteorite. We clearly detect the bandshift on all features after irradiation. We note that, no matter the dose, the relative band intensity is modified by irradiation, with bands below 500 cm^{-1} (above 20 μm) getting stronger compared to the one at 524 cm^{-1} (19.08 μm).

We studied the relation of the bandshift with the ion fluence on the 524 cm^{-1} (19.08 μm) band (bottom panel of Fig. 3). We fitted the variation of the peak position (PP) with an equation PP = AP + BS*exp(-σ*F), where AP is the asymptotic position at high irradiation, BS is the asymptotic band shift value, F is the ion fluence and σ is the cross section. We found values AP = 516±1 cm^{-1}, BS = 7.6±1 cm^{-1}, and $\sigma=(6\pm2)x10^{-17}$ cm^{2}. We obtained values of correlation coefficient $r^{2} = 0.99$ and reduced $\chi^{2} = 0.34$.

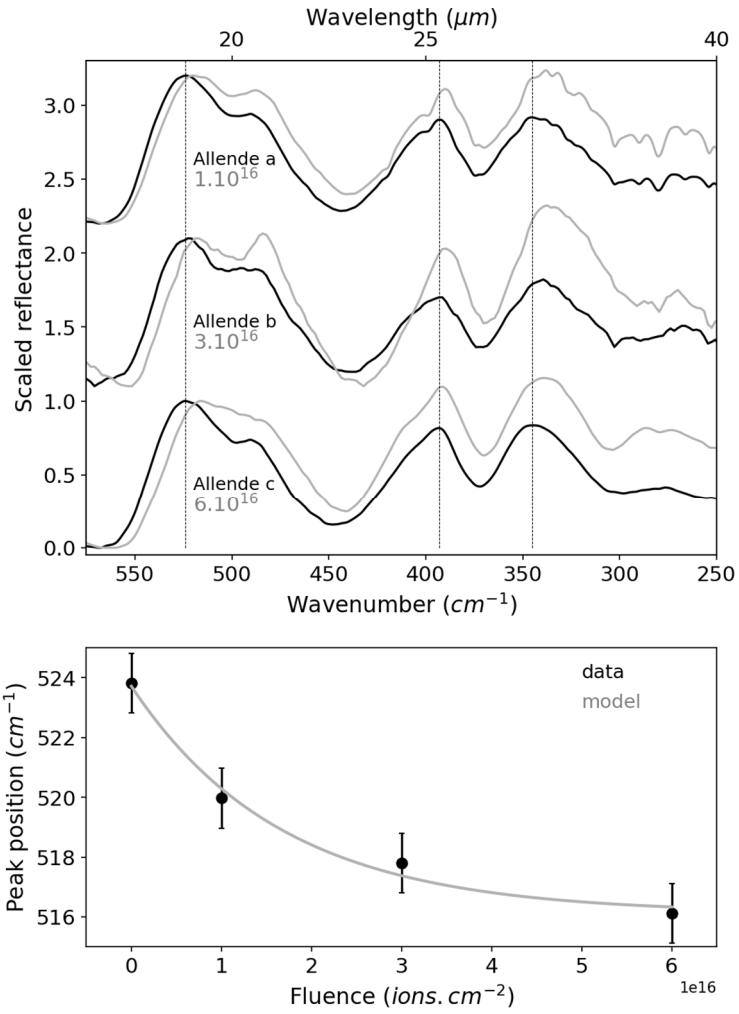

Fig. 3. Irradiation-induced bandshift is an efficient process. Top: Three Allende pellets measured in FIR before (black curves) and after (grey) irradiation at different doses (1, 3, and $6x10^{16}$ He^+/cm^2 at 40 keV). The spectra are normalized and shifted for clarity. The peak position before irradiation are highlighted by vertical lines. **Bottom:** Spectral shift of the 524 cm^{-1} band in Allende as a function of the ion fluence, along with an exponential fit.

4. Discussion

4.1 Detectability of the irradiation-induced spectral shifts by remote sensing observations

Based on the laboratory evidence of the redshift of IR silicate bands upon irradiation, we explored the possibility of detecting irradiation effects through the remote sensing observations of asteroids, using the bandshift as a proxy. In the top panel of Fig. 4 we display the observed MIR and FIR peak positions for a number of carbonaceous chondrites, before and after irradiation. The peak positions are determined both by the composition of the main minerals and by irradiation. Fortunately, different IR bands provide different proxies of the irradiation process, because they probe different surface layers. Combining the peak

positions of at least two bands as in Fig. 4 helps to disentangle the compositional variations from the irradiation effects. A spectral resolution of at least 10 cm^{-1} seems to be necessary to clearly detect the various spectral shifts produced by ion irradiation.

The separation between the spectral trend linked to the original composition of the meteorites and the irradiation trend is even clearer if the whole IR spectrum is considered. In the bottom panel of Fig. 4, we show the results of the Principal Component Analysis (PCA) of the whole spectral dataset (in the range 100-1200 cm^{-1}, 8.33-100 µm). A simple 2-components PCA is able to separate the experimental points into four main sectors, and thus to easily distinguish anhydrous from hydrated chondrites, and irradiated from unirradiated samples. Similar results are obtained by other clustering methods such as hierarchical clustering or multidimensional scaling (not shown here). The good detection of the irradiation trend by the clustering methods is probably due to the fact that not only the peak positions are affected by irradiation but also the general shape and width of all the IR bands. This demonstrates that measuring a large IR spectral range is a key point for detecting the irradiation effects.

The spectral modifications produced by irradiation proceed rapidly. The irradiation-induced spectral shift increases with increasing ion fluence (see Fig. 3), approaching asymptotic values for fluences above $6x10^{16}$ He^{+}/cm^{2} at 40 keV, which corresponds to a timescale of the order of ~10^{4} years in the inner Solar System (Brunetto et al. 2014). The use of the laboratory fluences to estimate an astrophysical timescale is justified by the fact that in our experiments we used an ion flux of ~10^{13} ions/(sec cm^{2}) that is low enough to statistically avoid an overlapping of the ion tracks (typically less than 10 nm in diameter) during the relaxation of the thermal spikes (typically less than 10 ps in time). A potential dependence of the spectral shift and the corresponding timescale on the ion energy cannot be excluded, and we consider this as an interesting subject for future studies.

Experiments and microscopic analyses suggest that the damage induced by He implantation may be responsible for the spectral modifications of the silicate bands observed in our irradiation experiments (Leroux et al. 2019). The implantation of solar wind ions has been identified in Itokawa grains as a major source of stress in the lattice of the original crystalline structure (Keller and Berger 2014; Thompson et al. 2014). In particular, the implanted He creates bubbles and vesicles at the end of the ion tracks, and significant damage all along the irradiated layers (Noguchi et al. 2014). Previous ion irradiation experiments (Brucato et al. 2004) showed that ion irradiation of olivine produces an amorphization at high dose, and the authors provided a dependence of the amorphization stage with the ion fluence. Comparing our fluence values with those reported in the litterature (Brucato et al. 2004), we estimate that the maximum He fluence we used in our experiments would correspond to a degree of damage in the irradiated layers (about 300 nm penetration depth, (Brunetto et al. 2014)) that is about 75% of complete amorphization (see Appendix A for comparison between the penetration depths of ions and photons). We infer that a similar ion-induced surface damage process is taking place on Itokawa and on our meteorites. The efficiency of space weathering in modifying IR optical properties suggests the possibility of detecting this process via IR remote sensing even on relatively young asteroid surfaces.

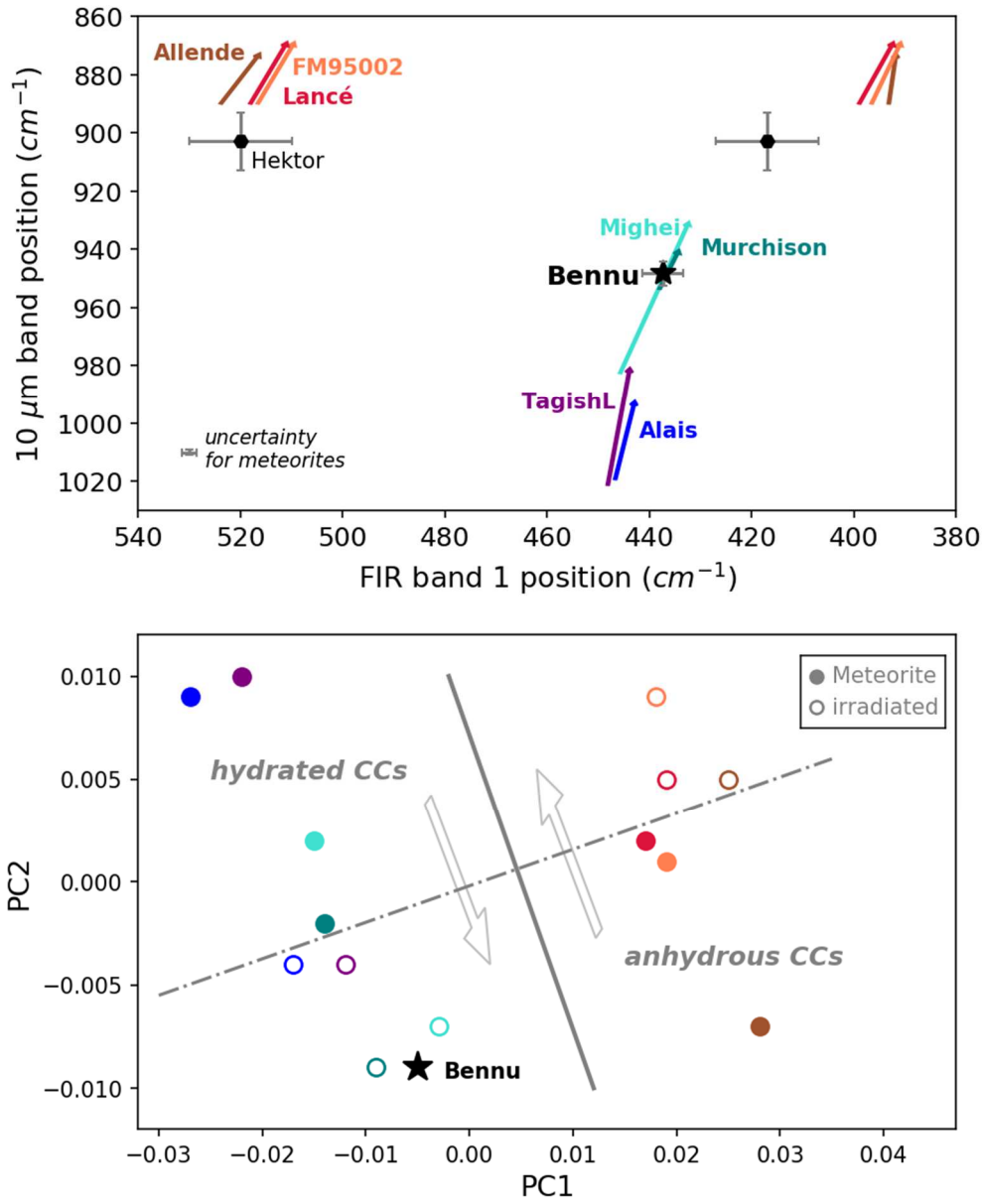

Fig. 4. Comparing spectral parameters of laboratory irradiated meteorites and asteroid observations. Top: MIR and FIR peak positions of carbonaceous chondrites compared to asteroids 101955 Bennu (observed by OTES instrument onboard OSIRIS-REx/NASA (Hamilton et al. 2019)) and 624 Hektor (observed by the IRS instrument on Spitzer (Emery et al. 2006)). The colored arrows describe the space weathering effect (the direction goes from unaltered to irradiated) for each meteorite (Allende, Lancé, Frontier Mountain 95002, Mighei, Alais, Tagish Lake, and Murchison). As shown in Figs. 1-3, Allende, Lancé, and FM95002 have two bands in the 380-540 cm^{-1} region; so does Hektor. The Murchison data are from the chip. The spectral changes are a function of the ion fluence (see Fig. 3). To focus on the effect of different compositions, we include here only meteorites irradiated with exactly the same ion fluence. A Murchison pellet sample, irradiated at lower fluence, provided qualitative similar results. It will be worth comparing the effects of irradiation on different surface preparations in a further dedicated study. **Bottom:** PC1 and PC2 scores from a principal component analysis performed on the combined MIR and FIR spectra (and baseline corrected, as presented in Fig. 2) of Bennu and the studied CCs. The PC1 and PC2 are not

linked to a specific mineralogy, but they rather represent two convenient axes containing the majority of the spectral information. They allow to quickly visualize the spread of our dataset, while reducing its dimensionality. The meteorites data have been resampled to Bennu's resolution for better comparison. Full and open circles are for the measurements before and after irradiation respectively. The color code is the same as the top panel. The arrows give the direction of irradiation. The lines are drawn to highlight the four sectors: unaltered and irradiated hydrated or anhydrous CCs.

Mid-IR and Far-IR spectra have previously been observed on asteroids by telescopes Spitzer (Emery et al. 2006) and IRTF (Vernazza et al. 2010). MIR and FIR spectra are currently being measured on asteroid (101955) Bennu by the OTES instrument (Christensen et al. 2018; Hamilton et al. 2019) onboard the OSIRIS-REx sample return mission (NASA) and will soon be observed by the MIRI instrument (Rieke et al. 2015) of the James Webb Space Telescope (JWST, NASA/ESA). The irradiation-induced spectral shifts are not detectable in IRTF observations because of poor signal to noise ratio (SNR) and spectral resolution (sampling worse than 12 cm^{-1} at 10 µm), while they are in principle detectable both by the IRS instrument onboard Spitzer and the OTES instrument onboard OSIRIS-REx. In the case of IRS the spectral resolution was $R = \lambda/\Delta\lambda \sim 64\text{-}128$ and the sampling was about 6.25 cm^{-1} at 10 µm, while in the case of OTES the spectral sampling was 8.66 cm^{-1} across the entire spectrum.

4.2 The cases of Bennu and Hektor

The top panel of Fig. 4 includes the peak positions observed for the near-Earth asteroid (101955) Bennu (Hamilton et al. 2019) and the Trojan asteroid (624) Hektor (Emery et al. 2006). Thanks to its proximity to the asteroid, the SNR of the Bennu observation by OTES was about five times better than the SNR of the Hektor observation by IRS (especially in the FIR), which explains the smaller error bars for Bennu in Fig. 4. For comparison, the SNR in our laboratory measurements was about 2000-5000 depending on the spectral range, **i.e.,** at least five times better than OTES. Bennu is reported in the PCA analysis of the bottom panel of Fig. 4, while the lower SNR of Hektor's FIR spectrum does not allow a reliable principal component analysis.

The first OTES observations of Bennu, obtained during the spacecraft approach phase (Hamilton et al. 2019), provide an interesting test for the use of IR spectra of lab-irradiated carbonaceous chondrites to detect space weathering. Previous ground-based observations of Bennu in the 0.4-2.4 spectral range (Clark et al. 2011) suggested CI- and CM-type chondrites as possible spectral matches for the asteroid. In the first observations performed by the OVIRS instrument onboard OSIRIS-REx in the near-IR spectral range, Bennu showed a clear 2.7 µm hydration band similar to the feature detected in aqueously altered CM1 and CM2 chondrites (Hamilton et al. 2019). In terms of mid- and far-IR peak positions observed by OTES (top of Fig. 4), the spectrum of Bennu clearly belongs to the group characterized by the presence of hydrated minerals, as found by (Hamilton et al. 2019). The IR peak positions of Bennu are particularly close to the irradiated CM chondrites. Looking in more detail, the PCA reinforces the closeness of Bennu with the lab-irradiated CMs, since its point clearly lies in the sector of the irradiated hydrated meteorites.

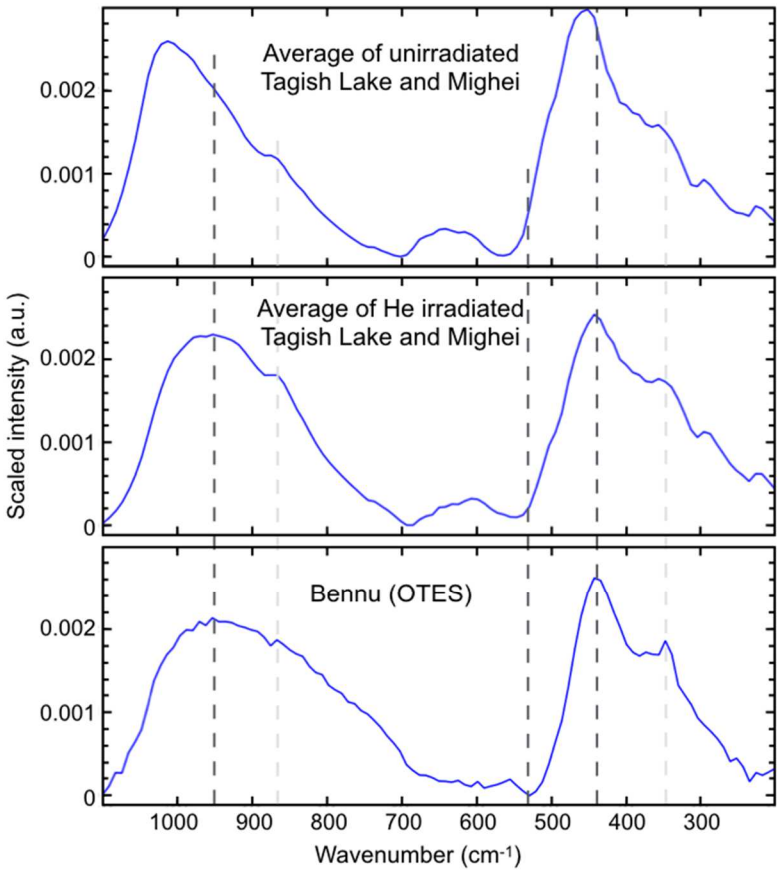

Fig. 5. The spectrum of Bennu compared with unirradiated and irradiated CCs. A linear combination of irradiated CM Mighei and irradiated C2 Tagish Lake meteorites (middle panel) provides a better qualitative match of the average spectrum of Bennu (bottom (Hamilton et al. 2019)) than the combination of the unirradiated samples (top). The average of the two meteorites is chosen here simply as an example to illustrate the effect of irradiation on the specific features of their hydrated minerals, rather than attempting to find the best analog of Bennu. The peak positions of the main features of Bennu are highlighted by vertical dashed lines. Each spectrum has been normalized to its total intensity.

The proximity of Bennu with the irradiated hydrated meteorites is confirmed by a visual inspection of the spectra (Fig. 5). Although none of the studied meteorites provides a perfect match to Bennu's spectrum, the resemblance of Bennu's spectra with those of irradiated CM Mighei, CM Murchison and potentially C2 Tagish Lake (both virgin and irradiated) is remarkable. Noticeable differences between Bennu and the considered meteorites remain in the right shoulder of the 10-µm feature, on the M-O-H bending region around 600-650 cm^{-1}, and on the absence of the 290 cm^{-1} feature in Bennu's spectrum (see also the discussion by (Hamilton et al. 2019). The irradiation effects seem to reduce some of these discrepancies. Most importantly, the irradiation significantly improves the match with the positions of all the reststrahlen bands (in particular the bands at ~950 cm^{-1} and ~440 cm^{-1}) and the Christiansen features (see for instance the improved match of the ~530 cm^{-1} feature), as well as the overall shape of the spectrum. A spectral combination of different irradiated meteorites would get even closer to Bennu in the PCA space. However, the main goal here is not to find the best meteorite match for Bennu, but rather to stress the effect of irradiation on the

specific features of the hydrated minerals. The notable match of the diagnostic peak positions of Bennu with those of irradiated meteorites suggests that the surface of Bennu may have recorded the effects of space weathering. If different regions with different degrees of space weathering were present on Bennu, their detection will be possible using OTES data in the near future by more detailed OSIRIS-REx observations, and eventually by the in-depth laboratory studies of the returned samples.

Differently from the case of Bennu, the points relative to Hektor in Fig. 4 are close to those of the anhydrous unirradiated meteorites. This agrees with what has been previously found (Emery et al. 2006), that olivines dominate the crystalline fraction of Hektor's surface minerals. It is interesting to observe that the peak positions for Hektor are blue-shifted with respect to those of the carbonaceous chondrites of our study (in particular the 11-μm band of olivine). This evidence confirms that none of these meteorites provides a good match of Hektor's spectrum and that the olivines on Hektor are probably richer in Mg than those found in the matrix of Allende, Lancé and FM95002, as it can be deduced based on literature data showing the relation between peak positions and Fo numbers (Hamilton 2010). Our results suggest that Hektor's surface has probably suffered less solar wind irradiation than Bennu, which would be in agreement with the dynamical properties of the two asteroids. Considering that the solar wind flux decreases as the square of the distance from the Sun, in the past ten million years (Walsh et al. 2019) a Trojan asteroid like Hektor (semimajor axis a=5.26 AU) must have accumulated an irradiation dose at least 20 times smaller than a near-Earth asteroid like Bennu (semimajor axis a=1.13 AU).

The example of Bennu suggests that irradiation effects may be present also on the primitive near-Earth asteroid (162173) Ryugu. The space weathering of Ryugu has been discussed in the context of visible and near-IR observations by Hayabusa2 (Sugita et al. 2019; Kitazato et al. 2019), but unfortunately the TIR instrument is not able to detect the MIR-FIR spectral shifts that we measured on irradiated samples. A direct and unambiguous detection of space weathering on Ryugu surface materials will have to wait for the sample return and analysis in 2021.

Will it be possible to detect space weathered surfaces using the JWST? The instrument MIRI has good chances to do so, thanks to its excellent spectral resolution capabilities. The medium resolution spectrometer of MIRI can reach R ~ 2500, a value which would be largely enough to detect the spectral bandshifts induced by irradiation. However, the detection of irradiation effects would still need an adequate signal to noise ratio. Values of SNR > 100-200 (or at least similar to the OTES SNR) seem to be absolutely necessary to unambiguously detect irradiation effects in the spectral range of MIRI. This can probably be achieved by rebinning the data to a lower spectral resolution to increase the SNR.

5. Conclusions

Spectra collected in the laboratory from virgin and irradiated meteorites indicate that a large IR spectral range is essential to recognize irradiation effects in remote sensing data. Due to their high spectral resolution IR instruments, the new generations of space missions and space telescopes open the way to a clear and unambiguous spectral detection of the space

weathering effects on asteroid surfaces. Observations by OSIRIS-REx are now being conducted and future observations by JWST are currently planned in the light of the cycle one proposal to be requested in early 2020. We stress the possibility of detecting space weathering effects with JWST observations, because IR investigation of irradiated surfaces may have broader implications than the study of asteroids. High-quality IR spectra of many unprotected surfaces in the Solar System are - or will soon be - available, from Mercury to the Trans-Neptunian region. As IR spectral variations upon irradiation are less ambiguous than in the VIS-NIR, they are a more reliable source of information to assess the irradiation history of surfaces, and to provide constraints of surface age and geological processes independent from dynamical studies.

Acknowledgements

The meteorite samples were kindly provided by the Natural History Museum of Vienna, the Vatican Observatory, J. Brucato, D. Cruikshank, and L. Folco. We are grateful to F. Capitani, A. Celeste, and C. Sandt for their precious help with the bolometer measurements at SOLEIL, and to P. Boiardi for useful suggestions on the manuscript. We warmly thank R.D. Hanna and M.S. Thompson for constructive reviews and discussions. PCA analysis was performed in Quasar (https://quasar.codes) using the Orange Spectroscopy toolbox (Toplak et al. 2017). The irradiations were performed using the INGMAR setup, a joint IAS-CSNSM (Orsay, France) facility funded by the P2IO LabEx (ANR-10-LABX-0038) in the framework Investissements d'Avenir (ANR-11-IDEX-0003-01). The MIR micro-spectroscopy measurements were supported by grants from Region Ile-de-France (DIM-ACAV) and SOLEIL. We thank J.P. Bibring for supporting the FIR spectroscopic activities at SOLEIL. This work has been funded by the Centre National d'Etudes Spatiales (CNES-France, Hayabusa2 mission and OSIRIS-REx mission) and by the ANR project CLASSY (Grant ANR-17-CE31-0004-02) of the French Agence Nationale de la Recherche.

SUPPLEMENTARY MATERIALS

Appendix A: detection of space weathering

The detectability of space weathering by reflectance spectral measurements is a function of the photon wavelength and of the surface optical properties, because it requires that the photons probe mainly the weathered layer of the upper surface. In the case of the slow solar wind, the irradiated layer is thinner than 1 µm (Noguchi et al. 2014; Brunetto et al. 2014). From the spectroscopic studies of minerals and meteorites, it is known that the VIS-NIR spectral region is characterized by the presence of weak absorptions, with typical values of $k=10^{-4}$-10^{-2} for the imaginary index (Roush 2003; Brunetto et al. 2007). In these conditions, photons interact with the surface materials in a volume scattering regime (Salisbury 1993), probing layers from tens to hundreds of µm thick, which are deeper than the penetration depth of solar wind ions. In the reflectance measurements of an irradiated surface, the emerging light would thus bring mixed information of both altered and unaltered layers, in a relative ratio which depends in a non-linear way on the absorption coefficient.

On the contrary, the mid-IR (MIR, 2.5-17 µm) and far-IR (FIR, 17-100 µm) spectral ranges show strong absorptions (typical values of k=0.1-10 at the center of the absorption bands (Roush 2003; Zeidler et al. 2015)), that are due to the high values of the band strengths of the fundamental molecular vibrations of minerals. At the centre of the bands, the main MIR and FIR mineral absorptions probe a much shallower surface layer than VIS-NIR photons. For instance, considering the optical constants of serpentine (Mooney and Knacke 1985), the penetration depth of visible photons would be higher than 40 µm, whereas it would be about 2 µm for photons in the 2.7 µm OH-band, and it would drop to less than 1 µm for photons from the center of the main MIR and FIR reststrahlen bands. Of course these values change according to the optical properties of the considered target material, but in any case the emerging photons in the main IR bands tend to be the most sensitive to the irradiated layers and are good potential proxies to detect weathered surfaces. The 9-50 µm range, in particular, seems promising because it includes a number of strong absorption bands due to silicates, each one of them providing an independent proxy of the surface. A similar behaviour of wavelength-dependent absorption difference was reported in experimental studies of silica-coated basalts (Kraft et al. 2003), which showed that silica coatings can be spectrally detected first in the areas of high absorption, while low absorption areas are only spectrally modified with thicker coatings. An example of detection of irradiation effects using different spectral parameters is reported in Fig. A1.

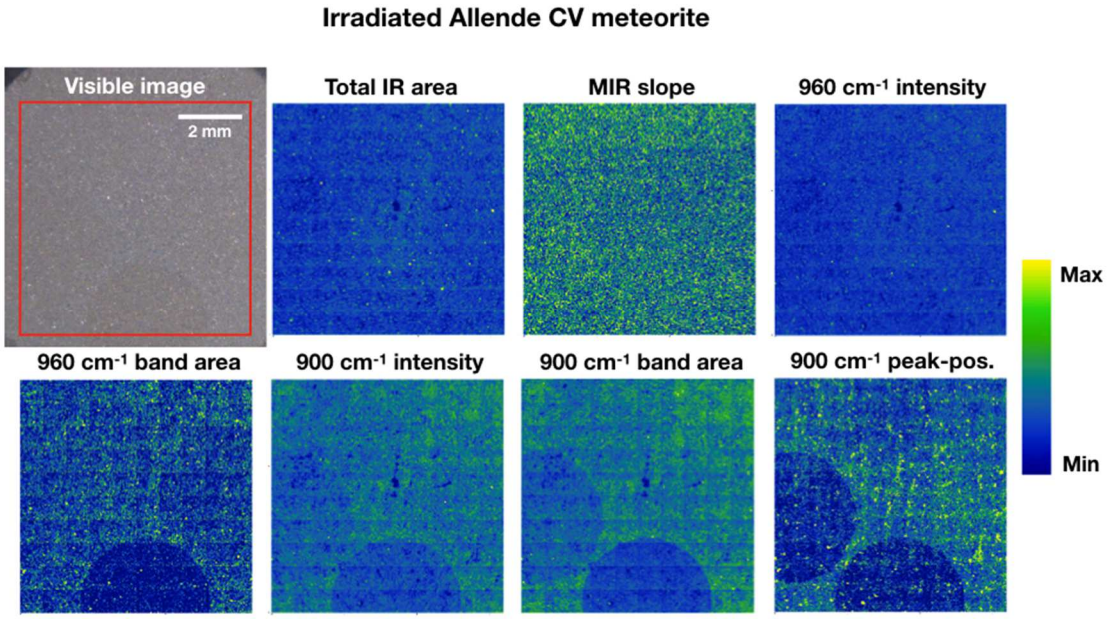

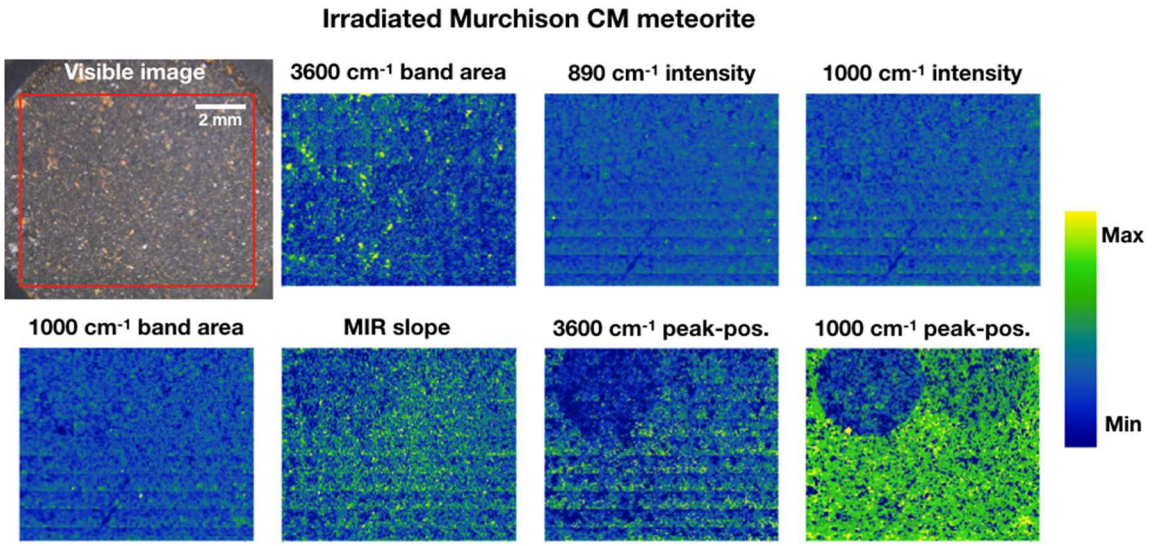

Fig. A1. Spectral imaging of irradiated meteorite pellets. A visible image and seven IR spectral parameters maps are reported for laboratory-irradiated carbonaceous chondrites (CV Allende and CM Murchison in this example, top and bottom respectively). The samples were pressed pellets (7 tons, diameter 13 mm) of meteorite powder (unconstrained grain size), and four irradiation areas (diameter 4 mm) were produced at the surface of each sample, using different ions and fluences (Allende: 5E14 and 1E16 He^+/cm^2, and 1E14 and 2E15 Ar^+/cm^2. Murchison: 2E15 and 3E16 He^+/cm^2, and 5E14 and 6E15 Ar^+/cm^2). Ion irradiation produces an IR spectral shift of the main silicates reststrahlen bands (bottom right map for each meteorite). The IR bandshift induced by irradiation can be used as an irradiation-meter: two irradiation areas (highest fluences for He and Ar) can be easily detected on each meteorite by tracing the peak position of the main silicate band (900 cm^{-1} for Allende, 1000 cm^{-1} for Murchison). These irradiation circles are hardly detected by other spectral parameters that use photons in the visible range (upper left visible images) or photons in weaker IR bands. The two other irradiation circles produced at lower fluences are more difficult to recognize, suggesting these fluences are at the detection limit of irradiation effects.

According this this interpretation, we would expect reduced spectral changes from irradiation in the volume scattering areas of low absorption, most particularly in the Christiansen feature areas and transparency regions between the restrahlen bands, and from Figs. 1-3 we see that this is clearly not the case. However, the imaginary index is still quite high in mid- and far-IR regions of low absorption, e.g. k=0.3-1 for serpentine around the Christiansen and transparency features (Mooney and Knacke 1985), and in any case it is higher than the values of k in the visible and near-IR ranges. Other factors that probably need to be considered are how the optical constants are changing within the irradiated layer and how physical changes (vesicularity, lattice stress, etc.) may be affecting the penetration depth. To resolve these observations, future studies will need to combine results from (micro-)spectroscopy and high-resolution transmission electron microscopy of the irradiated layers (Leroux et al. 2019).

References

Beck, P., A. Garenne, E. Quirico, L. Bonal, G. Montes-Hernandez, F. Moynier, and B. Schmitt. 2014. “Transmission Infrared Spectra (2–25µm) of Carbonaceous Chondrites (CI, CM, CV–CK, CR, C2 Ungrouped): Mineralogy, Water, and Asteroidal Processes.” *Icarus* 229 (February): 263–77.

Binzel, Richard P., Andrew S. Rivkin, J. Scott Stuart, Alan W. Harris, Schelte J. Bus, and Thomas H. Burbine. 2004. “Observed Spectral Properties of near-Earth Objects: Results for Population Distribution, Source Regions, and Space Weathering Processes.” *Icarus* 170 (2): 259–94.

Bonal, L., R. Brunetto, P. Beck, E. Dartois, Z. Dionnet, Z. Djouadi, J. Duprat, et al. 2015. “Visible-IR and Raman Microspectroscopic Investigation of Three Itokawa Particles Collected by Hayabusa: Mineralogy and Degree of Space Weathering Based on Nondestructive Analyses.” *Meteoritics & Planetary Science*. https://doi.org/10.1111/maps.12496.

Brucato, J. R., G. Strazzulla, G. Baratta, and L. Colangeli. 2004. “Forsterite Amorphisation by Ion Irradiation: Monitoring by Infrared Spectroscopy.” *Astronomy & Astrophysics. Supplement Series* 413 (2): 395–401.

Brunetto, R., C. Lantz, Z. Dionnet, F. Borondics, A. Aléon-Toppani, D. Baklouti, M. A. Barucci, et al. 2018. “Hyperspectral FTIR Imaging of Irradiated Carbonaceous Meteorites.” *Planetary and Space Science* 158 (September): 38–45.

Brunetto, R., C. Lantz, D. Ledu, D. Baklouti, M. A. Barucci, P. Beck, L. Delauche, et al. 2014. “Ion Irradiation of Allende Meteorite Probed by Visible, IR, and Raman Spectroscopies.” *Icarus* 237 (July): 278–92.

Brunetto, Rosario, Mark J. Loeffler, David Nesvorn\`y, Sho Sasaki, and Giovanni Strazzulla. 2015. “Asteroid Surface Alteration by Space Weathering Processes.” *Asteroids Iv*, 597–616.

Brunetto, Rosario, Ted L. Roush, Anna Cinzia Marra, and Vincenzo Orofino. 2007. “Optical Characterization of Laser Ablated Silicates.” *Icarus* 191 (1): 381–93.

Brunetto, R., P. Vernazza, S. Marchi, M. Birlan, M. Fulchignoni, V. Orofino, and G. Strazzulla. 2006. “Modeling Asteroid Surfaces from Observations and Irradiation Experiments: The Case of 832 Karin.” *Icarus*. https://doi.org/10.1016/j.icarus.2006.05.019.

Christensen, P. R., V. E. Hamilton, G. L. Mehall, D. Pelham, W. O’Donnell, S. Anwar, H. Bowles, et al. 2018. “The OSIRIS-REx Thermal Emission Spectrometer (OTES) Instrument.” *Space Science Reviews* 214 (5): 87.

Clark, Beth Ellen, Richard P. Binzel, Ellen S. Howell, Edward A. Cloutis, Maureen Ockert-Bell, Phil Christensen, Maria Antonietta Barucci, et al. 2011. “Asteroid (101955) 1999 RQ36: Spectroscopy from 0.4 to 2.4µm and Meteorite Analogs.” *Icarus* 216 (2): 462–75.

Emery, J. P., D. P. Cruikshank, and J. Van Cleve. 2006. “Thermal Emission Spectroscopy (5.2–38 µm) of Three Trojan Asteroids with the Spitzer Space Telescope: Detection of Fine-Grained Silicates.” *Icarus* 182 (2): 496–512.

Hamilton, V. E., N. M. Abreu, P. A. Bland, H. C. Connolly, R. D. Hanna, D. S. Lauretta, and D. L. Schrader. 2018. “Spectral Classification of Ungrouped Carbonaceous Chondrites II: Parameters and Comparison to Independent Measures.” In . https://ui.adsabs.harvard.edu/abs/2018LPI....49.1753H.

Hamilton, V. E., A. A. Simon, P. R. Christensen, D. C. Reuter, B. E. Clark, M. A. Barucci, N. E. Bowles, et al. 2019. “Evidence for Widespread Hydrated Minerals on Asteroid (101955) Bennu.” *Nature Astronomy* 3 (4): 332–40.

Hamilton, Victoria E. 2010. “Thermal Infrared (vibrational) Spectroscopy of Mg–Fe Olivines: A Review and Applications to Determining the Composition of Planetary Surfaces.” *Geochemistry: Exploration, Environment, Analysis* 70 (1): 7–33.

Hapke, Bruce. 2001. “Space Weathering from Mercury to the Asteroid Belt.” *Journal of Geophysical Research* 106 (E5): 10039–73.

Jäger, C., F. J. Molster, and J. Dorschner. 1998. “Steps toward Interstellar Silicate

Mineralogy. IV. The Crystalline Revolution." *Astronomy*. http://adsabs.harvard.edu/full/1998A%26A...339..904J.
Keller, Lindsay P., and Eve L. Berger. 2014. "A Transmission Electron Microscope Study of Itokawa Regolith Grains." *Earth, Planets and Space* 66 (1): 71.
Kitazato, K., R. E. Milliken, T. Iwata, M. Abe, M. Ohtake, S. Matsuura, T. Arai, et al. 2019. "The Surface Composition of Asteroid 162173 Ryugu from Hayabusa2 near-Infrared Spectroscopy." *Science* 364 (6437): 272–75.
Kraft, Michael D., Joseph R. Michalski, and Thomas G. Sharp. 2003. "Effects of Pure Silica Coatings on Thermal Emission Spectra of Basaltic Rocks: Considerations for Martian Surface Mineralogy." *Geophysical Research Letters* 30 (24). https://agupubs.onlinelibrary.wiley.com/doi/abs/10.1029/2003GL018848.
Lantz, C., R. Brunetto, M. A. Barucci, E. Dartois, J. Duprat, C. Engrand, M. Godard, D. Ledu, and E. Quirico. 2015. "Ion Irradiation of the Murchison Meteorite: Visible to Mid-Infrared Spectroscopic Results." *Astronomy & Astrophysics. Supplement Series* 577: A41.
Lantz, C., R. Brunetto, M. A. Barucci, S. Fornasier, D. Baklouti, J. Bourçois, and M. Godard. 2017. "Ion Irradiation of Carbonaceous Chondrites: A New View of Space Weathering on Primitive Asteroids." *Icarus*. https://doi.org/10.1016/j.icarus.2016.12.019.
Lazzarin, M., S. Marchi, L. V. Moroz, R. Brunetto, S. Magrin, Paolo Paolicchi, and G. Strazzulla. 2006. "Space Weathering in the Main Asteroid Belt: The Big Picture." *Astrophysical Journal Letters* 647 (2): L179.
Leroux, H., F. de la Peña, C. Le Guillou, C. Lantz, and R. Brunetto. 2019. "Spectral and Microstructural Modifications of Olivine Under Ion Irradiation." *LPI Contributions* 2157 (July). https://ui.adsabs.harvard.edu/abs/2019LPICo2157.6261L.
Loeffler, M. J., C. A. Dukes, and R. A. Baragiola. 2009. "Irradiation of Olivine by 4 keV He + : Simulation of Space Weathering by the Solar Wind." *Journal of Geophysical Research* 114 (E3): 953.
Marchi, S., R. Brunetto, S. Magrin, M. Lazzarin, and D. Gandolfi. 2005. "Space Weathering of near-Earth and Main Belt Silicate-Rich Asteroids: Observations and Ion Irradiation Experiments." *Astronomy & Astrophysics. Supplement Series* 443 (3): 769–75.
Mooney, T., and R. F. Knacke. 1985. "Optical Constants of Chlorite and Serpentine between 2.5 and 50 μm." *Icarus* 64 (3): 493–502.
Nagao, Keisuke, Ryuji Okazaki, Tomoki Nakamura, Yayoi N. Miura, Takahito Osawa, Ken-Ichi Bajo, Shintaro Matsuda, et al. 2011. "Irradiation History of Itokawa Regolith Material Deduced from Noble Gases in the Hayabusa Samples." *Science* 333 (6046): 1128–31.
Nakamura, Tomoki, Takaaki Noguchi, Michael E. Zolensky, and Masahiko Tanaka. 2003. "Mineralogy and Noble-Gas Signatures of the Carbonate-Rich Lithology of the Tagish Lake Carbonaceous Chondrite: Evidence for an Accretionary Breccia." *Earth and Planetary Science Letters* 207 (1): 83–101.
Nesvorný, David, Robert Jedicke, Robert J. Whiteley, and Željko Ivezić. 2005. "Evidence for Asteroid Space Weathering from the Sloan Digital Sky Survey." *Icarus* 173 (1): 132–52.
Noguchi, Takaaki, Makoto Kimura, Takahito Hashimoto, Mitsuru Konno, Tomoki Nakamura, Michael E. Zolensky, Ryuji Okazaki, et al. 2014. "Space Weathered Rims Found on the Surfaces of the Itokawa Dust Particles." *Meteoritics & Planetary Science* 49 (2): 188–214.
Noguchi, T., T. Nakamura, M. Kimura, M. E. Zolensky, M. Tanaka, T. Hashimoto, M. Konno, et al. 2011. "Incipient Space Weathering Observed on the Surface of Itokawa Dust Particles." *Science* 333 (6046): 1121–25.
Pieters, C. M., E. M. Fischer, O. Rode, and A. Basu. 1993. "Optical Effects of Space Weathering: The Role of the Finest Fraction." *Journal of Geophysical Research*. https://doi.org/10.1029/93je02467.
Rieke, George H., G. S. Wright, T. Böker, J. Bouwman, L. Colina, Alistair Glasse, K. D. Gordon, et al. 2015. "The Mid-Infrared Instrument for the James Webb Space Telescope, I: Introduction." *Publications of the Astronomical Society of the Pacific* 127 (953): 584.
Roush, Ted L. 2003. "Estimated Optical Constants of the Tagish Lake Meteorite." *Meteoritics*

& Planetary Science 38 (3): 419–26.
Salisbury, John W., Dana M. D'Aria, and Eugene Jarosewich. 1991. "Midinfrared (2.5–13.5 μm) Reflectance Spectra of Powdered Stony Meteorites." *Icarus* 92 (2): 280–97.
Salisbury, J. W. 1993. "Mid-Infrared Spectroscopy: Laboratory Data." *Remote Geochemical Analysis: Elemental and Mineralogical Composition* 618.
Sasaki, S., K. Nakamura, Y. Hamabe, E. Kurahashi, and T. Hiroi. 2001. "Production of Iron Nanoparticles by Laser Irradiation in a Simulation of Lunar-like Space Weathering." *Nature* 410 (6828): 555–57.
Schmitt, Bernard, Philippe Bollard, Alexandre Garenne, Damien Albert, Lydie Bonal, and Olivier Poch. 2018. "SSHADE: The European Solid Spectroscopy Database Infrastructure." In *European Planetary Science Congress*. Vol. 12. https://wiki.sshade.eu/_media/sshade/documentation/sshade_poster_els-mai2018_a0.pdf.
Strazzulla, G., E. Dotto, R. Binzel, R. Brunetto, M. A. Barucci, A. Blanco, and V. Orofino. 2005. "Spectral Alteration of the Meteorite Epinal (H5) Induced by Heavy Ion Irradiation: A Simulation of Space Weathering Effects on near-Earth Asteroids." *Icarus* 174 (1): 31–35.
Sugita, S., R. Honda, T. Morota, S. Kameda, H. Sawada, E. Tatsumi, M. Yamada, et al. 2019. "The Geomorphology, Color, and Thermal Properties of Ryugu: Implications for Parent-Body Processes." *Science* 364 (6437): 252.
Thompson, Michelle S., Roy Christoffersen, Thomas J. Zega, and Lindsay P. Keller. 2014. "Microchemical and Structural Evidence for Space Weathering in Soils from Asteroid Itokawa." *Earth, Planets and Space* 66 (1): 1–10.
Toplak, M., G. Birarda, S. Read, C. Sandt, S. M. Rosendahl, L. Vaccari, J. Demšar, and F. Borondics. 2017. "Infrared Orange: Connecting Hyperspectral Data with Machine Learning." *Synchrotron Radiation News* 30 (4): 40–45.
Vernazza, P., R. P. Binzel, A. Rossi, M. Fulchignoni, and M. Birlan. 2009. "Solar Wind as the Origin of Rapid Reddening of Asteroid Surfaces." *Nature* 458 (7241): 993–95.
Vernazza, P., B. Carry, J. Emery, J. L. Hora, D. Cruikshank, R. P. Binzel, J. Jackson, J. Helbert, and A. Maturilli. 2010. "Mid-Infrared Spectral Variability for Compositionally Similar Asteroids: Implications for Asteroid Particle Size Distributions." *Icarus* 207 (2): 800–809.
Vernazza, P., J. Castillo-Rogez, P. Beck, J. Emery, R. Brunetto, M. Delbo, M. Marsset, et al. 2017. "DIFFERENT ORIGINS OR DIFFERENT EVOLUTIONS? DECODING THE SPECTRAL DIVERSITY AMONG C-TYPE ASTEROIDS." *AJS; American Journal of Sociology* 153 (2): 72.
Vernazza, P., D. Fulvio, R. Brunetto, J. P. Emery, C. A. Dukes, F. Cipriani, O. Witasse, et al. 2013. "Paucity of Tagish Lake-like Parent Bodies in the Asteroid Belt and among Jupiter Trojans." *Icarus* 225 (1): 517–25.
Walsh, K. J., E. R. Jawin, R-L Ballouz, O. S. Barnouin, E. B. Bierhaus, H. C. Connolly, J. L. Molaro, et al. 2019. "Craters, Boulders and Regolith of (101955) Bennu Indicative of an Old and Dynamic Surface." *Nature Geoscience* 12 (4): 242–46.
Zeidler, S., H. Mutschke, and Th Posch. 2015. "TEMPERATURE-DEPENDENT INFRARED OPTICAL CONSTANTS OF OLIVINE AND ENSTATITE." *The Astrophysical Journal* 798 (2): 125.